Resonance factorized scattering and roaming trajectories

2006 J. Phys. A: Math. Gen. 39 12847

(http://iopscience.iop.org/0305-4470/39/41/S08)

INSTITUTE OF PHYSICS PUBLISHING JOURNAL OF PHYSICS A: MATHEMATICAL AND GENERAL

J. Phys. A: Math. Gen. **39** (2006) 12847–12861 doi:10.1088/0305-4470/39/41/S08

Resonance factorized scattering and roaming trajectories*

Al B Zamolodchikov[1]

Département de Physique de l'Ecole Normale Supérieure, 24 rue Lhomond, F-75231 Paris Cedex 05, France

Received 8 February 2006, in final form 16 July 2006
Published 27 September 2006
Online at stacks.iop.org/JPhysA/39/12847

Abstract

A simple resonance factorized scattering theory is studied by the thermodynamic Bethe ansatz technique. While the limiting ultraviolet central charge is predicted to be $c = 1$, at the intermediate distances the model reveals the characteristic pattern of the trajectory which flows down wandering about several different fixed points. The field theory nature of the model considered is not completely clear, however.

PACS numbers: 11.80.−m, 05.50.+q, 11.25.Hf

1. Preliminaries

The thermodynamic Bethe ansatz (TBA) [1, 2] is proved to be a useful technique in studying 2D integrable models of relativistic field theory. It is applied in the situation when the relativistic factorized scattering theory (RFST) is known and allows the extraction of certain off-mass-shell characteristics, including the ultraviolet (UV) parameters of the background field theory. This provides an explicit and direct link between the RFST and the conformal field theory (CFT) which governs the UV behaviour of the corresponding integrable model. Several RFSTs, previously conjectured as scattering theories of important integrable models, were verified in this way [2–4]. On the other hand, many RFSTs can be constructed, which are completely consistent from the scattering theory's point of view, but they lack any known field theory interpretation. In the present paper one particular example is considered. We shall see that even very simple RFST can hide rather rich and interesting off-mass-shell pattern.

* This paper first appeared in preprint form in 1991; it is included here as the Guest Editors feel it is of great interest for the theme of this special issue, and they wish to take this opportunity to circulate its results more widely to the community.

[1] Permanent address: Institute of Theoretical Experimental Physics B. Cheremushkinskaya 25, 117259, Moscow, Russia.

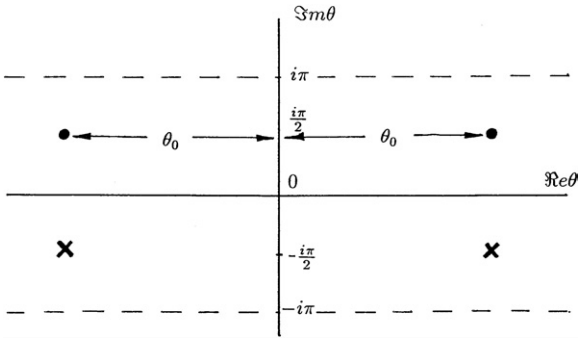

Figure 1. Zeros (•) and poles (×) of the scattering amplitude (1). The structure in the rest part of the θ-plane follows from the periodicity $S(\theta + 2i\pi) = S(\theta)$.

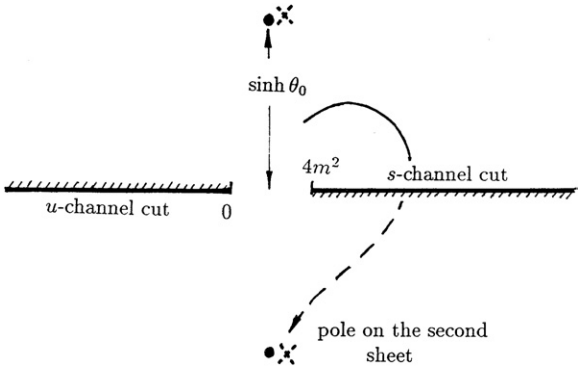

Figure 2. Analytic structure in the s-plane. The poles (dashed crosses) on the second sheet are misplaced a bit for transparency; in fact, they are just under the zeros.

2. The scattering theory

The RFST we are going to consider here contains a single stable particle, which we choose to be the neutral boson of mass m. On the same footing one can consider it as the fermion, changing the sign of the scattering amplitude below. The RFST is completely defined by the two-particle scattering amplitude

$$S(\theta) = \tanh\left(\frac{\theta - \theta_0}{2} - \frac{\mathrm{i}\pi}{4}\right)\tanh\left(\frac{\theta + \theta_0}{2} - \frac{\mathrm{i}\pi}{4}\right), \tag{1}$$

where $\theta = \theta_1 - \theta_2$ is the rapidity difference of two colliding particles and θ_0 is a real parameter. This amplitude satisfies the usual requirements of crossing symmetry and unitarity

$$S(\theta) = S(\mathrm{i}\pi - \theta), \qquad S(\theta)S(-\theta) = 1 \tag{2}$$

and exhibits in the physical strip $0 \leqslant \mathrm{Im}\,\theta < \pi$ two zeros at $\theta = \mathrm{i}\pi/2 \pm \theta_0$ (figure 1). The analytic structure in the s-channel invariant $s = 2m^2(1 + \cosh\theta)$ is presented in figure 2. As usual for the diagonal scattering of neutral particles we have the two-sheet Riemann surface with square-root threshold branch points 0 and $4m^2$, which originate the u-channel cut $(-\infty, 0]$ and the s-channel one $[4m^2, \infty)$. Two zeros are located at $s = 2m^2 \pm 2im^2\sinh\theta_0$ on the physical sheet, while on the second (unphysical) sheet there are two resonance poles at the same positions (figure 2).

3. Motivations

There are basically two motivations to study the scattering theory above. First, it can be considered as a massive version of the Goldstone resonance scattering theory suggested in [5] in connection with the massless integrable field theory interpolating between the tricritical Ising fixed point and the critical Ising one. In that case the massless particles were the Goldstone fermions respecting nonlinear realization of spontaneously broken supersymmetry and the resonance pole was interpreted as a manifestation of unstable Higgs boson. Suppose now some perturbation of this field theory, which explicitly breaks the SUSY and provides the Goldstone particles with a small mass m, while preserving the integrability. Then the scattering theory described above (with $\mathrm{e}^{\theta_0} \ll 1$) seems natural; the Higgs boson mass scale is $M^2 = m^2\,\mathrm{e}^{\theta_0}$.

The second motivation becomes clear after one rewrites the scattering amplitude (1) in the following form:

$$S(\theta) = \frac{\sinh\theta - \mathrm{i}\cosh\theta_0}{\sinh\theta + \mathrm{i}\cosh\theta_0}. \tag{3}$$

This expression bears a strong resemblance to the scattering amplitude in the sinh-Gordon model, i.e. the model of 2D scalar field $\varphi(x)$ with the action

$$A_{\mathrm{shG}} = \int \left[\frac{1}{2}\,(\partial_a\varphi)^2 - 2\mu\cosh\beta\varphi\right]\mathrm{d}^2x, \tag{4}$$

where β is the dimensionless coupling constant. The second term in action (4) can be viewed as the perturbation of the CFT of free massless scalar field by the operator $\mathrm{e}^{\beta\varphi} + \mathrm{e}^{-\beta\varphi}$ of negative dimension

$$\Delta = -\beta^2/8\pi; \tag{5}$$

the dimensional coupling μ is therefore $\mu \sim [\mathrm{mass}]^{1+\beta^2/8\pi}$. Like the sine-Gordon model, model (4) is massive and integrable [6]. The corresponding RFST is just the theory of single neutral massive particle with the scattering amplitude [6, 7]

$$S_{\mathrm{shG}}(\theta) = \frac{\sinh\theta - \mathrm{i}\sin\gamma}{\sinh\theta + \mathrm{i}\sin\gamma}, \tag{6}$$

where constant γ is related to the sinh-Gordon coupling β as follows [6, 7]:

$$\gamma = \frac{\beta^2/8}{1 + \beta^2/8\pi}. \tag{7}$$

Comparing equations (3) and (6) one observes that the scattering theory (3) can be viewed as an analytic continuation of the sinh-Gordon RFST (6) to complex values of the coupling constant γ:

$$\gamma = \frac{\pi}{2} \pm \mathrm{i}\theta_0. \tag{8}$$

This observation will be used below for speculations.

4. The TBA equation

Since we are dealing with the diagonal RFST (1), the derivation of the corresponding TBA system goes along the standard lines. We shall not discuss here the details of the TBA technique, referring to papers [1–3] for general definitions and derivations. In brief, TBA describes the free energy of an integrable relativistic field system at finite temperature T or,

equivalently, the ground state energy $E(R)$ of the same system living on the space circle of finite length $R = 1/T$. The finite-temperature effects are described by a set of pseudoenergies ε_a, one for each specie of stable particles in the RFST spectrum. The pseudoenergies $\varepsilon_a(\theta)$ are real functions of rapidity; roughly speaking, quantities $1/(1 + \exp(\varepsilon_a(\theta))$ characterize filling of the particle states at rapidity θ.

In the scattering theory introduced above (equation (1)), corresponding to single stable particle we have single pseudoenergy $\varepsilon(\theta)$, which determines the finite size ground state energy

$$E(R) = -\frac{m}{2\pi}\int L(\theta)\cosh\theta\,\mathrm{d}\theta \tag{9}$$

and satisfies the following nonlinear integral equation:

$$-mR\cosh\theta + \varepsilon + \frac{1}{2\pi}\varphi * L = 0, \tag{10}$$

where star $*$ denotes the rapidity convolution. Note that in the RFST (1) we have $S(0) = -1$ and therefore the TBA system (9), (10) is of 'fermionic' type [2, 3]. In equations (9) and (10) the notation

$$L(\theta) = \log(1 + \mathrm{e}^{-\varepsilon(\theta)}) \tag{11}$$

is used. Information about the scattering theory (1) is carried by the kernel $\varphi(\theta)$:

$$\begin{aligned}\varphi(\theta) = -\mathrm{i}\frac{\partial}{\partial\theta}\log S(\theta) &= \frac{4\cosh\theta_0\cosh\theta}{\cosh 2\theta + \cosh 2\theta_0}\\ &= \frac{1}{\cosh(\theta+\theta_0)} + \frac{1}{\cosh(\theta-\theta_0)}.\end{aligned} \tag{12}$$

The UV limit in the TBA equation (10) corresponds to $R \to 0$ where one expects the behaviour to be governed by the limiting UV CFT of the background field theory. For the Casimir energy (9) CFT predicts [8] $E(R) \sim \pi c_{\mathrm{UV}}/6R$, where c_{UV} is the central charge characteristic for the UV CFT. At moderate distances it is convenient to define the effective central charge $c_{\mathrm{eff}}(R)$ [3],

$$E(R) = -\frac{\pi c_{\mathrm{eff}}(x)}{6R}, \tag{13}$$

which is a function of the circle length R or, more conveniently, of the variable

$$x = \log\frac{mR}{2}. \tag{14}$$

For the UV calculations it is convenient to perform an overall rapidity shift in equation (10) and rewrite it in the form

$$-\mathrm{e}^{\theta} - \mathrm{e}^{2x}\,\mathrm{e}^{-\theta} + \varepsilon + \frac{1}{2\pi}\varphi * L = 0 \tag{15}$$

with the effective central charge given by

$$c_{\mathrm{eff}}(x) = \frac{6}{\pi^2}\int \mathrm{e}^{\theta}L(\theta)\,\mathrm{d}\theta. \tag{16}$$

Here it is probably safe to keep temporarily the same notation $L(\theta)$ for the shifted function (11). In the UV limit $x = -\infty$, it is possible to neglect the term $\mathrm{e}^{2x}\,\mathrm{e}^{-\theta}$ in the TBA equation (15). This results in the scale invariant reduced TBA equation, for which one has a solution with the limiting value $\lim_{\theta\to-\infty}\varepsilon(\theta) = \infty$. Standard central charge calculation [2, 3] then gives for $c_{\mathrm{UV}} = c_{\mathrm{eff}}(-\infty)$,

$$c_{\mathrm{UV}} = 1. \tag{17}$$

Slightly more subtle consideration about the next UV corrections is performed in appendix A. It results in the following leading $x \to -\infty$ behaviour of the effective central charge:

$$c_{\text{eff}}(x) = 1 - \frac{3\left(\theta_0^2 + \pi^2/4\right)}{2x^2} + O\left(\frac{1}{x^3}\right). \tag{18}$$

Note that this form of UV behaviour differs essentially from the usual perturbative expansion of the Casimir energy in fractional powers of R [2–4]. In the case of sinh-Gordon field theory, which corresponds to purely imaginary θ_0, the origin of these logarithmic UV corrections can be traced to the contribution of the sinh-Gordon zero mode fluctuations. In appendix B the zero mode contribution to the Casimir energy is carried out in the UV limit. For the leading logarithmic correction we find exactly the same expression (18) (with θ_0 imaginary). Besides the logarithmic zero mode terms one also expects the usual power-like perturbative UV corrections.

An interesting structure connected with the TBA equation (10) is worth mentioning. Usually, it is more convenient to study the UV properties of TBA equations representing them in the universal functional form [9]. In particular the structure of the UV perturbative expansions is readily observed in this way. With the kernel (12), the functional form reads as a finite difference functional relation for the function $Y(\theta) = \exp(-\varepsilon(\theta))$:

$$Y\left(\theta + \frac{\mathrm{i}\pi}{2}\right) Y\left(\theta - \frac{\mathrm{i}\pi}{2}\right) = (1 + Y(\theta + \theta_0))(1 + Y(\theta - \theta_0)). \tag{19}$$

Restricting the entire function $Y(\theta)$ at the lattice $\theta_{mn} = \Theta + m\theta_0 + \mathrm{i}\pi n/2$ (where $m, n \in Z$ and Θ is an arbitrary origin of the lattice) in the complex θ-plane and denoting $Y_{mn} = Y(\theta_{mn})$, we arrive at the two-dimensional nonlinear discrete equation

$$Y_{m,n+1} Y_{m,n-1} = (1 + Y_{m+1,n})(1 + Y_{m-1,n}). \tag{20}$$

It is interesting to note the resemblance of the functional equation (19) to the analogous functional form corresponding to the infinite TBA chains suggested in [10] for integrable asymptotically free field theories. In that case there was an infinite number of entire functions $Y_m(\theta)$ satisfying the following functional system:

$$Y_m\left(\theta + \frac{\mathrm{i}\pi}{2}\right) Y_m\left(\theta - \frac{\mathrm{i}\pi}{2}\right) = (1 + Y_{m+1}(\theta))(1 + Y_{m-1}(\theta)) \tag{21}$$

Being restricted to the string of complex values $\theta_n = \Theta + \mathrm{i}\pi n/2, n \in Z$, this system again becomes the discrete equation (20). Thus the system (20) seems rather important and universal. Since it appears in the context of integrable field theory, it is natural to expect it to be also integrable in some sense.

5. Qualitative considerations

Turn to qualitative discussion of the TBA equation (10). We are going to follow the development of function $L(\theta)$ with the variable x decreasing continuously from the massive region $x > 0$ to the deep UV limit $x \to -\infty$. Peculiarities of equation (10) are most prominent when $\theta_0 \gg 1$. In this case the kernel (12) exhibits two far separated bumps at $\theta = \pm\theta_0$, as shown in figure 3 (for $\theta_0 = 50$). This implies that at $x \sim 1$ the convolution term in equation (10) does not influence the behaviour of the solution, which follows therefore the free fermion pattern, i.e. $L(\theta) = \log\left(1 + \mathrm{e}^{-mR\cosh\theta}\right)$. At $x > 0$ we have the bell-shaped $L(\theta)$ (figure 4(*a*)), characteristic for the massive region, where c_{eff} falls exponentially with R. Then, at $x < 0$,

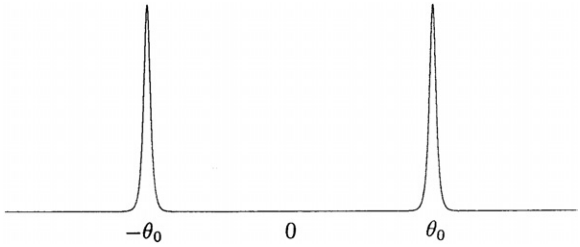

Figure 3. Kernel (12) at $\theta_0 = 50$.

$L(\theta)$ develops a plateau of height $\log 2$ in the region $x < \theta < -x$ (figure 4(b)), i.e. the pattern characteristic for the free neutral fermion UV behaviour. As x decreases the plateau broadens and $c_{\rm eff}(x)$ saturates the characteristic free fermion limit $c_{\rm eff} = 1/2$. It goes on this way until at $x \sim -\theta_0/2$ two plateau edges interact via the kernel in equation (10) (figure 1(c)). $c_{\rm eff}$ deviates here from $1/2$. Since at $\theta_0 \gg 1$ the edges are far separated, we readily realize that the interaction can be described by two separate interacting integral equations for two separate pseudoenergies $\varepsilon_1(\theta) = \varepsilon(\theta + \theta_0/2)$ and $\varepsilon_2(\theta) = \varepsilon(\theta - \theta_0/2)$. In fact, the resulting system coincides with the system of two TBA equations related in [5] to the integrable trajectory interpolating between the tricritical Ising and critical Ising fixed points. Therefore, as x goes down through the region $x \sim -\theta_0/2$, the effective central charge switches from $c_{\rm eff} = 1/2$ to the characteristic tricritical Ising value $c_{\rm eff} = 7/10$, the interpolating curve $c_{\rm eff}(x)$ following in this region almost exactly (at $\theta_0 \gg 1$) the curve of [5]. At x well below $-\theta_0/2$, in the rapidity regions $\theta_0 + x < \theta < -x$ and $x < \theta < -\theta_0 - x$ we have approximately constant solutions of the two coupled TBA equations. Function $L(\theta)$ develops here two higher plateaux of height $2\log\left(2\cos\frac{\pi}{5}\right)$, which rise above the main plateau in between (figure 1(d)). The central charge is approximately constant $c_{\rm eff} = 7/10$ until at $x \sim -\theta_0$ these two higher plateaux join at the centre $\theta \sim 0$ (figure 1(e)). Here the central region interacts via the kernel (12) with both the edges and we can simulate equation (10) introducing three separate pseudoenergies to describe the two edges and the central region. These three are again governed by the coupled TBA system, suggested in [5] to interpolate between the $\mathcal{M}_5$ and $\mathcal{M}_4$ minimal model fixed points. Therefore at $x \sim -\theta_0$ we expect a new switch from $c_{\rm eff} = 7/10$ to $c_{\rm eff} = 4/5$, which again follows nearly the integrable $\mathcal{M}_5 \to \mathcal{M}_4$ trajectory. At $-3\theta_0/2 < x < -\theta_0$ we observe $L(\theta)$ with three plateaux (figure 1(f)), right and left ones of height $\log 3$ and the central plateau of height $\log 4$, all rising above the intermediate level $2\log(2\cos\pi/5)$. The plateaux broaden with x decreasing and collide at $x \sim -3\theta_0/2$ (figure 1(g)), where we expect again a jump from $c_{\rm eff} = 4/5$ to $c_{\rm eff} = 6/7$, i.e. the value characteristic for the $\mathcal{M}_6$ fixed point. This goes on with x going down to $-\infty$. Every time $x \sim -(p-2)\theta_0/2$, $p = 3, 4, 5, \ldots$, a switch occurs from the $\mathcal{M}_p$ central charge $c_{\rm eff} = 1 - 6/(p(p+1))$ to the $\mathcal{M}_{p+1}$ value $c_{\rm eff} = 1 - 6/((p+1)(p+2))$, the function $L(\theta)$ acquiring more and more complicated form with multiple plateaux. Few more Gothic examples are plotted in figures 4(h)–(k). Like figures 4(a)–(g), they are obtained by numerical integration of equation (10) (see the next section).

Finally, for $\theta_0 \gg 1$ we expect the function $c_{\rm eff}(x)$ to have a staircase behaviour with the steps of height $c_{\rm eff} = 1 - 6/(p(p+1))$ inside every interval $-(p-2)\theta_0/2 < x < -(p-3)\theta_0/2$, $p = 3, 4, 5, \ldots$. Clearly, the difference between the neighbouring steps becomes small at $x \to -\infty$ and the staircase picture is slurred. Note that on average the heights and width of the steps are consistent with the asymptotic behaviour (18) (recall that θ_0 is large).

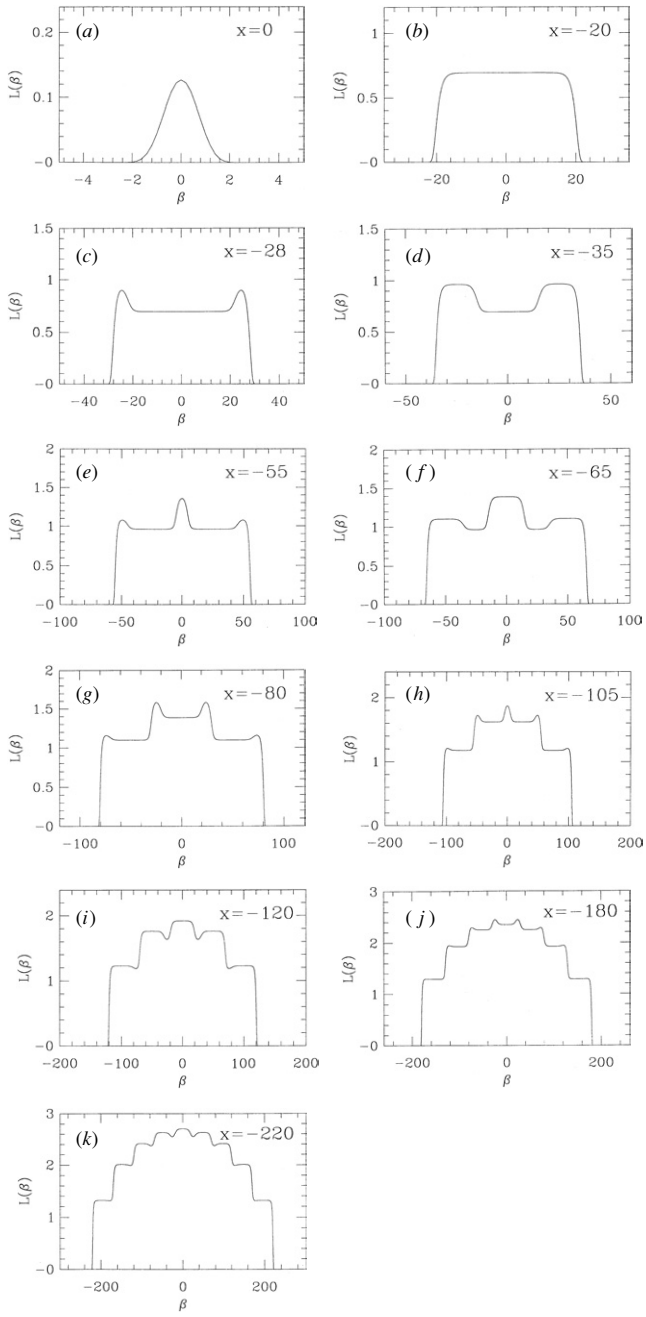

Figure 4. (*a*) Function $L(\theta)$ in the massive region $x \sim 0$ ($\theta_0 = 50$). (*b*) At $x > -\theta_0$ interaction is absent. $L(\theta)$ follows the free fermion pattern ($\theta_0 = 50$). (*c*) Resonance interaction between the edge particles at $x \sim -\theta_0/2$ ($\theta_0 = 50$). (*d*) Three plateaux pattern at $-\theta_0 < x < -\theta_0/2$ ($\theta_0 = 50$). (*e*) $x \sim -\theta_0$ ($\theta_0 = 50$). Central particles interact with the plateau edges. (*f*) Central and border plateaux broaden when x decreases in the interval $-3\theta_0/2 < x < -\theta_0$ ($\theta_0 = 50$). (*g*) $x \sim -3\theta_0/2$ ($\theta_0 = 50$). (*h*) Example of $L(\theta)$ at $\theta_0 = 50$ and $x = -105$. (*i*) Example of $L(\theta)$ at $\theta_0 = 50$ and $x = -120$. (*j*) Example of $L(\theta)$ at $\theta_0 = 50$ and $x = -180$. (*k*) Example of $L(\theta)$ at $\theta_0 = 50$ and $x = -220$. In pictures (*a*)–(*k*) the arguments θ and functions $L(\theta)$ are denoted β and $L(\beta)$ respectively.

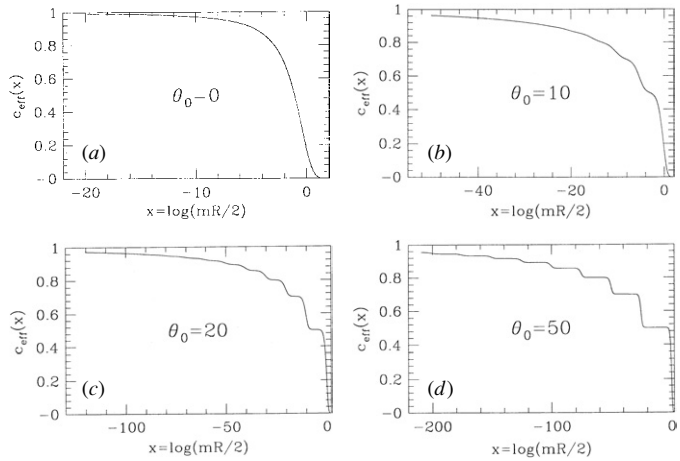

Figure 5. (*a*) Effective central charge behaviour at $\theta_0 = 0$. Result of numerical solution of TBA equation (10). (*b*) $c_{\text{eff}}(x)$ at $\theta_0 = 10$. (*c*) $c_{\text{eff}}(x)$ at $\theta_0 = 20$. (*d*) Staircase pattern of $c_{\text{eff}}(x)$ at $\theta_0 = 50$.

6. Numerical calculations

TBA equation (10) was solved numerically by iterations of the function $L(\theta)$, which was represented as a set of values at discrete rapidity points separated by $\Delta\theta = 0.2$. Some numerical examples of $L(\theta)$ are presented in figure 4; they were already discussed in the previous section. Few plots of the effective central charge $c_{\text{eff}}(x)$ are drawn in figure 5 for $\theta_0 = 0, 10, 20$ and 50. While at θ_0 we observe a smooth curve interpolating between $c_{\text{eff}} = 1$ at $x \to -\infty$ and $c_{\text{eff}} = 0$ at $x > 2$, the staircase pattern speculated above becomes more and more prominent as θ_0 increases. At $\theta_0 = 50$ (figure 5(*d*)) one can clearly recognize as much as eight steps, the highest being of height $21/22$ and corresponding to $\mathcal{M}_{11}$ central charge. In fact, figure 5(*d*) implies even more distinct steps at $x < -200$. However, in this region $c_{\text{eff}}(x)$ was not carried out numerically because of deterioration of the iterative procedure.

7. Roaming trajectories

Patterns of figures 5(*b*)–(*d*) give rise to a remarkable interpretation in terms of the renormalization group (RG) flows. It was observed in [11] that in the RG space there is an infinite sequence of fixed points, corresponding to the conformal minimal models $\mathcal{M}_p$, $p = 3, 4, \ldots$. These points are characterized by the central charge values $c_p = 1 - 6/(p(p+1))$ and at $p \to \infty$ are condensed (in the RG sense) near the limiting fixed point $\mathcal{M}_\infty$ with $c = 1$. Every two successive fixed points $\mathcal{M}_p$ and $\mathcal{M}_{p-1}$ are connected by the RG trajectory $\mathcal{M}_p \to \mathcal{M}_{p-1}$. This trajectory corresponds to massless interpolating field theory, which has the $\mathcal{M}_p$ CFT asymptotic in the UV limit, while the massless infrared region is controlled by the CFT model $\mathcal{M}_{p-1}$. The whole trajectory is drawn from the UV fixed point by the relevant $\mathcal{M}_p$ operator Φ_{13}. In the infrared limit the trajectory is attracted to $\mathcal{M}_{p-1}$ by the irrelevant scalar field Φ_{31} of the infrared minimal CFT. This pattern, which is drawn conventionally in figure 6, was demonstrated in [11, 12] by the perturbative RG analysis, reliable at p large. It is commonly believed that the qualitative picture holds for all $p > 3$ (at $\mathcal{M}_3$ the attracting operator Φ_{31} is substituted by the descendant CFT field $\bar{T}T$ [13, 5]) until finally at $\mathcal{M}_3$ the operator Φ_{13} generates a trajectory with massive infrared behaviour (figure 6).

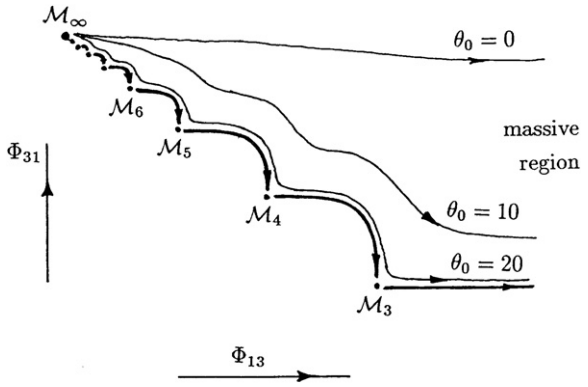

Figure 6. Sequence of $\mathcal{M}_p$ fixed points connected by integrable interpolating trajectories $\mathcal{M}_p \to \mathcal{M}_{p-1}$ is drawn schematically. At $\theta_0 \to \infty$ the wandering trajectory flows arbitrary close near the sequence.

The characteristic staircases of figures 5(*b*)–(*d*) are suggestive for the trajectories flowing near the succession of $\mathcal{M}_p$ fixed points, as it is pictured schematically in figure 6. Corresponding to the parameter θ_0 we have a one-dimensional variety of roaming trajectories of this kind. Every trajectory starts at the limiting fixed point $\mathcal{M}_\infty$, in consistency with the UV central charge (17). At θ_0 large enough the trajectory flows very close to the fixed points $\mathcal{M}_p$, spending approximately the same fraction $\theta_0/2$ of the RG 'time' x near each one and jumping in between successively from one fixed point $\mathcal{M}_p$ to the next one $\mathcal{M}_{p-1}$ approximately along the interpolating trajectory $\mathcal{M}_p \to \mathcal{M}_{p-1}$. The larger the value of θ_0 the closer the approach of the trajectory to the fixed points and the nearer the paths in between to the massless flows $\mathcal{M}_p \to \mathcal{M}_{p-1}$. The time $\theta_0/2$ near each point becomes very large and the transitions of the effective central charge $c_{\text{eff}}(x)$ follow the same form as for the massless interpolations, just as it was speculated above qualitatively. Since at p large the fixed points $\mathcal{M}_p$ are very close to each other in the RG space, the picture of distinct successive transitions between the fixed points is slurred at $x \to -\infty$.

It follows from the results of [14] that all the interpolating trajectories $\mathcal{M}_p \to \mathcal{M}_{p-1}$ are integrable. We observed, in addition, a one-parameter family of integrable wandering trajectories for which the succession of $\mathcal{M}_p \to \mathcal{M}_{p-1}$ flows is unified as the limiting $\theta_0 \to \infty$ trajectory.

It remains to be verified, however, that the picture above is consistent with the perturbative RG predictions, at least at $-x/\theta_0 \gg 1$, where the trajectory is near the large p fixed points $\mathcal{M}_p$.

8. The beta-function

The numerical data obtained in section 6 can be used to calculate the RG beta-functions along the corresponding RG trajectories. Instead of the scale parameter x we parameterize the trajectory with the 'coupling constant' parameter g and denote ϕ the corresponding tangential operator, which draws the field theory along the trajectory, i.e.,

$$\langle\phi\rangle_R = \frac{\pi}{6R}\frac{\partial c_{\text{eff}}}{\partial g}, \tag{22}$$

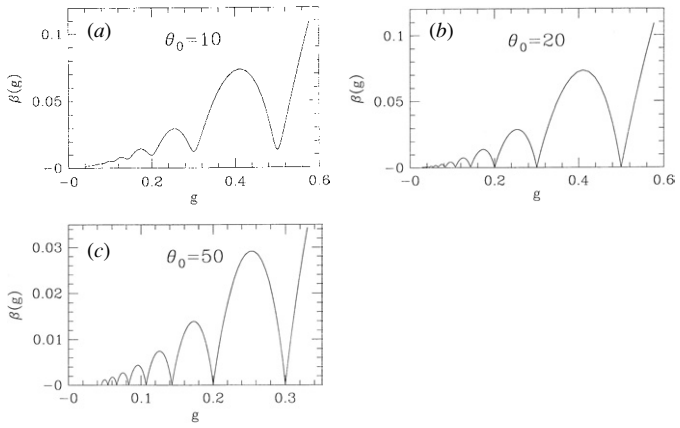

Figure 7. (*a*) RG beta-function along the trajectory $\theta_0 = 10$. It exhibits deeps near $g = 6/(p(p+1))$, $p = 3, 4, \ldots$. (*b*) Beta-function along the $\theta_0 = 20$ trajectory. (*c*) At $\theta_0 = 50$ $\beta(g)$ is indistinguishable from the sequence of beta-functions along the interpolating trajectories $\mathcal{M}_p \to \mathcal{M}_{p-1}$.

where $\langle \cdots \rangle_R$ is the expectation value in the TBA geometry, i.e. on the infinite cylinder of circumference R. Since $c_{\rm eff}$ is a monotonically decreasing function of the scale (see figures 5(*a*)–(*d*)), we can normalize the field ϕ as follows:

$$-\frac{6}{\pi}\langle\phi\rangle_{R=1} = 1. \tag{23}$$

Note that this norm is not necessarily the same as the norm in the RG metric introduced in [15] in terms of two-point correlation functions. It is clear, however, that the norm (23) is physically close to that determined by the metric of [15] and therefore it can be used for qualitative considerations. Normalizing g to be zero at the UV fixed point we find from equation (22)

$$g = c_{\rm UV} - c_{\rm eff}, \tag{24}$$

i.e. with the norm (23) the trajectory is parameterized by just the effective central charge. Differentiating this with respect to the scale parameter x we find

$$\beta(g) = -\frac{\partial c_{\rm eff}}{\partial x}. \tag{25}$$

Equations (24) and (25) give a parametric representation of the RG function $\beta(g)$.

In figures 7(*a*)–(*c*) the numerical results are pictured for $\theta_0 = 10$, 20 and 50. At $\theta_0 = 10$ (figure 7(*a*)) $\beta(g)$ exhibits a series of deeps near the values $g = 6/(p(p+1))$, $p = 3, 4, \ldots$, indicating the presence of fixed points nearby. In figure 7(*b*) ($\theta_0 = 20$) several first deeps (with $p < 6$) are already indistinguishable from zeros. The beta-function in between remains unchanged under further growth of θ_0 and in fact coincides with the beta-functions along the corresponding interpolating trajectories. What is changing when θ_0 increases further is that the higher deeps (corresponding to larger p) turn subsequently to zeros, the intermediate beta-function being stabilized at the corresponding interpolating shapes (figure 7(*c*)).

9. Complex dimensions?

To conclude we develop here few speculations about the formal analytic connection (8) between the resonance RFST (3) and the sinh-Gordon scattering theory. The sinh-Gordon

perturbation $e^{\beta\varphi} + e^{-\beta\varphi}$ consists of two free field exponentials. According to the two signs in equation (8) there are two possible continuations of each term, which result in four complex exponentials $U_\pm = \exp(\pm i\sqrt{8\pi}\alpha_+\varphi)$ and $V_\pm = \exp(\pm i\sqrt{8\pi}\alpha_-\varphi)$, where

$$\alpha_\pm = \frac{i\pi/2 \pm \theta_0}{\sqrt{\pi^2/4 + \theta_0^2}}, \qquad \alpha_+\alpha_- = -1. \tag{26}$$

From the CFT point of view these exponentials are scalar primary fields of complex conformal dimensions $\Delta_+ = \dim(U_\pm)$ and $\Delta_- = \dim(V_\pm)$:

$$\Delta_+ = \frac{\theta_0 + i\pi/2}{\theta_0 - i\pi/2}, \qquad \Delta_- = 1/\Delta_+. \tag{27}$$

Nevertheless, along the lines of [14] one can verify that under all the four exponential perturbations $U_\pm$ and $V_\pm$ the same infinite set of local integrals of motion survives. This means that formally every perturbation of the form

$$A = \int \left[\frac{1}{2}(\partial_\mu\varphi)^2 + \mu_+U_+ + \mu_-U_- + \nu_+V_+ + \nu_-V_-\right] d^2x \tag{28}$$

(where $\mu_\pm \sim (\text{mass})^{2-2\Delta_+}$ and $\nu_\pm \sim (\text{mass})^{2-2\Delta_-}$ are arbitrary coupling constants of complex dimensionality) is locally integrable. It is interesting to note that the formal perturbative expansion of the Casimir energy (or the effective central charge (13)) with the action (28) results in a series of the following form:

$$\sum_{m,n=0}^{\infty} F_{mn}(\mu_+\mu_-)^m(\nu_+\nu_-)^n R^{2(\omega_+m+\omega_-n)}, \tag{29}$$

where F_{mn} are the numerical coefficients determined by the corresponding perturbative integrals and $\omega_\pm = 2 - 2\Delta_\pm$. If action (28) is real, the perturbative expansion is also real and we have a series in the oscillating functions:

$$\sum_{m,n=0}^{\infty} G_{mn} \exp\left(\frac{2\pi^2(m+n)x}{\theta_0^2 + \pi^2/4}\right) \cos\left(\frac{4\pi(m-n)\theta_0(x - x_{mn})}{\theta_0^2 + \pi^2/4}\right), \tag{30}$$

where x was defined in equation (14) while G_{mn} and x_{mn} are the real constants. The main period of oscillations here is $\left(\theta_0^2 + \pi^2/4\right)/2\theta_0$. At $\theta_0 \gg 1$ this is just $\theta_0/2$, in agreement with the period observed above in the TBA considerations.

Apparently, the observations of the paper imply more questions than answers. The most annoying puzzle is the field theory background of the resonance RFST suggested in section 2. The action (28) would be an excellent candidate if it were not be apparently ill defined. Even being chosen real it by no means can be arranged bounded from below. Therefore, even if this action makes any sense (as the perturbative considerations suggest), its precise meaning should be specified.

Acknowledgments

Discussions with E Brézin, Vl S Dotsenko, V A Fateev and especially with S P Novikov and A B Zamolodchikov were very useful and encouraging.

Appendix A

Here we consider the TBA equation (15) in the limit $x \to -\infty$, having in mind to keep the logarithmic UV corrections to the effective central charge (16) while neglecting the

exponentially small in x (perturbative) contributions. Kernel (12) has the following Fourier transform:

$$\varphi(k) = \int \varphi(\theta)\, \mathrm{e}^{\mathrm{i}k\theta}\, \mathrm{d}\theta = \frac{2\pi \cos\theta_0 k}{\cosh(\pi k/2)}. \tag{A.1}$$

Expanding $\varphi(k)$ in powers of k

$$\frac{1}{2\pi}\varphi(k) = \sum_{n=0}^{\infty} (-)^n \frac{\varphi_{2n}}{(2n)!} k^{2n}, \tag{A.2}$$

where

$$\begin{aligned} \varphi_0 &= 1 \\ \varphi_2 &= \left(\theta_0^2 + \pi^2/4\right) \\ \varphi_4 &= \left(\theta_0^2 + \pi^2/4\right)\left(\theta_0^2 + 5\pi^2/4\right) \\ \varphi_6 &= \left(\theta_0^2 + \pi^2/4\right)\left(\theta_0^4 + 7\pi^2\theta_0^2/2 + 61\pi^4/16\right) \\ &\cdots. \end{aligned} \tag{A.3}$$

we can formally represent equation (15) as an infinite-order ordinary differential equation

$$\mathrm{e}^{\theta} + \mathrm{e}^{2x}\, \mathrm{e}^{-\theta} + \log(1 - \mathrm{e}^{-L(\theta)}) = \sum_{n=1}^{\infty} \frac{\varphi_{2n}}{(2n)!} L^{(2n)}(\theta), \tag{A.4}$$

where we denoted $L^{(n)}(\theta) = (\mathrm{d}/\mathrm{d}\theta)^n L(\theta)$.

If $x \to -\infty$ and the rapidity region $\theta - 2x \gg 1$ is considered, one can neglect $\mathrm{e}^{2x}\, \mathrm{e}^{-\theta}$ on the left-hand side of equation (A.4) and consider the reduced equation

$$\mathrm{e}^{\theta} + \log(1 - \mathrm{e}^{-L(\theta)}) = \sum_{n=1}^{\infty} \frac{\varphi_{2n}}{(2n)!} L^{(2n)}(\theta). \tag{A.5}$$

On the other hand, it is this region $y < \theta < \infty$; $y \sim x$, where the integral of equation (16) gains almost all its amount, leaving an exponentially small contribution for the rest region of integration. It is convenient to define the truncated version of integral (12), introducing the truncated effective central charge $c_{\mathrm{eff}}(x, y)$:

$$\frac{\pi^2}{6} c_{\mathrm{eff}}(x, y) = \int_y^{\infty} \mathrm{e}^{\theta} L(\theta)\, \mathrm{d}\theta. \tag{A.6}$$

Note that when $y \sim x$ or less, the truncated central charge becomes independent of y and in fact coincides with the total one $c_{\mathrm{eff}}(x)$ (of course, up to exponentially small contributions).

Obviously $c_{\mathrm{eff}}(x, y)$ satisfies the differential equation in y:

$$\frac{\pi^2}{6} \frac{\partial c_{\mathrm{eff}}(x, y)}{\partial y} = -\mathrm{e}^{-y} L(y). \tag{A.7}$$

One can verify directly that the following expression

$$\frac{\pi^2}{6} c_{\mathrm{eff}}(x, y) = -\frac{1}{2} \sum_{n=1}^{\infty} \frac{\varphi_{2n}}{(2n)!} \sum_{k=1}^{2n-1} (-)^k L^{(k)}(y) L^{(2n-k)}(y) - \int_0^{L(y)} \log(1 - \mathrm{e}^{-t})\, \mathrm{d}t - \mathrm{e}^{y} L(y) \tag{A.8}$$

formally solves equation (A.7) provided $L(y)$ satisfies equation (A.5). Moreover, since as $y \to +\infty$ the function $L(y)$ vanishes together with all its derivatives, we have from (A.8) $c_{\mathrm{eff}}(x, \infty) = 0$ and therefore expression (A.8) coincides with the integral (A.6).

Note that at $x \to -\infty$ and $\theta - 2x \gg \theta_0$ there are two qualitatively different rapidity regions in the TBA equation (15). In the region $\theta \sim \theta_0$ (the edge region), the non-local nature of the TBA equation is essential and all the derivative terms in formal expansion (A.5) are relevant. In contrast, at θ well below $-\theta_0$ (the central region) function $L(\theta)$ is large and slowly varying. To a certain logarithmic approximation one can neglect here the infinite sequence of higher derivative terms keeping a finite number of first ones. Now we are going to restrict ourselves to the leading logarithmic correction to $c_{\text{eff}}(x)$. In this case it is consistent to keep in equation (A.5) only the second-order derivative and only the first term in the expansion $\log(1 - \mathrm{e}^{-L}) = -\mathrm{e}^{-L} + \cdots$. In the central region we can also neglect the e^{θ} term on the rhs of equation (A.5) and deal with

$$\frac{\theta_0^2 + \pi^2/4}{2} L''(\theta) + \mathrm{e}^{-L(\theta)} = 0. \tag{A.9}$$

The truncated central charge (A.8) takes the following form in this approximation:

$$c_{\text{eff}}(x, y) = 1 + \frac{\frac{3}{2}\left(\theta_0^2 + \pi^2/4\right)}{\pi^2} (L'(\theta))^2 - \frac{6}{\pi^2}\, \mathrm{e}^{-L(y)}. \tag{A.10}$$

This expression is easily verified to be independent of y provided $L(y)$ satisfies equation (A.9). An appropriate solution to equation (A.9) in the central region is

$$L(\theta) = \log \frac{\sin^2 \lambda(\theta - a)}{\lambda^2\left(\theta_0^2 + \pi^2/4\right)}, \tag{A.11}$$

where λ and a are the parameters to be determined by the boundary conditions at $\theta \sim \theta_0$ and $\theta - 2x \sim \theta_0$. In the limit $x \to -\infty$ parameter λ tends to zero, while a becomes some x-independent constant a_0, which cannot be determined in our approximation and requires the solution of the whole equation (A.5) in the edge region $\theta \sim \theta_0$. Respecting the symmetry $\theta \to 2x - \theta$ of the TBA equation (15) we find

$$\lambda = \frac{\pi/2}{a_0 - x}. \tag{A.12}$$

Finally, substituting solution (A.11) we find the effective central charge (A.10) to the leading logarithmic approximation

$$c_{\text{eff}}(x) = 1 - \frac{6\lambda^2}{\pi^2}\left(\theta_0^2 + \pi^2/4\right) = 1 - \frac{\frac{3}{2}\left(\theta_0^2 + \pi^2/4\right)}{(a_0 - x)^2}. \tag{A.13}$$

Appendix B

Consider the sinh-Gordon model (4) on the infinite cylinder of circumference R. Since this field theory can be viewed as a perturbation of the free massless CFT, the leading UV behaviour of the Casimir energy $E(R) = \pi c_{\text{eff}}/6R$ is governed by the CFT central charge $\lim_{R\to 0} c_{\text{eff}} = 1$. At $R \to 0$ corrections are dominated by the fluctuations of the zero mode φ_0 of field φ. We shall see below that these fluctuations contribute non-perturbatively in the effective coupling constant $t = \mu R^{2\pi/(\pi-\gamma)}$. Contributions of the non-zero mode excitations are relatively suppressed by powers of t. The zero mode dynamics is governed by the Schrödinger equation with the $\cosh \beta\varphi_0$ potential. We arrive at the lowest eigenvalue problem for the hyperbolic Mathieu equation,

$$\left(-\frac{1}{2}\frac{\mathrm{d}^2}{\mathrm{d}\varphi_0^2} + 8\pi^2 t \cosh \beta\varphi_0\right) \Psi(\varphi_0) = \frac{\pi\epsilon}{6} \Psi(\varphi_0), \tag{B.1}$$

which we should inspect in the limit $t \to 0$. In equation (B.1) $\epsilon = 1 - c_{\rm eff}(t)$ and $\Psi(\varphi_0)$ is the ground state zero mode wavefunction.

At $t \to 0$ there is a central region in φ_0, where $|\varphi_0| \ll \beta^{-1} \log(\epsilon/(48\pi t))$, and one can neglect the potential term in equation (B.1). For the ground state eigenfunction we find here

$$\Psi(\varphi_0) = A \cos(p\beta\varphi_0), \tag{B.2}$$

where A is some normalization constant and

$$\epsilon = \frac{3\beta^2 p^2}{\pi}. \tag{B.3}$$

On the other hand, in the edge region $\varphi_0 \sim \beta^{-1} \log(\epsilon/(48\pi t))$ one can substitute $2\cosh\beta\varphi_0 = \mathrm{e}^{\beta\varphi_0}$ and deal with the Bessel equation:

$$\left(-\frac{1}{2}\frac{\mathrm{d}^2}{\mathrm{d}\varphi_0^2} + 4\pi^2 t\, \mathrm{e}^{\beta\varphi_0}\right)\Psi(\varphi_0) = \frac{\pi\epsilon}{6}\Psi(\varphi_0). \tag{B.4}$$

Appropriate solution, which decreases as $\varphi_0 \to \infty$, involves the modified Bessel function $K_\nu(z)$:

$$\Psi(\varphi_0) = B K_{2\mathrm{i}p}\left(\frac{4\pi}{\beta}\sqrt{2t}\,\mathrm{e}^{\beta\varphi_0/2}\right), \tag{B.5}$$

where B is an arbitrary wavefunction normalization. Solutions (B.2) and (B.5) match in the central region provided

$$p \log\frac{8\pi^2 t}{\beta^2} + \phi(p) = \frac{\pi}{2}, \tag{B.6}$$

where

$$\phi(p) = -\frac{\mathrm{i}}{2}\log\frac{\Gamma(1-2\mathrm{i}p)}{\Gamma(1+2\mathrm{i}p)}. \tag{B.7}$$

From equation (B.6) we find at $t \to 0$

$$p = \frac{\pi/2}{\log(8\pi^2 t/\beta^2) + 2C}, \tag{B.8}$$

where C is Euler's constant. Finally, we get

$$\epsilon = \frac{3\gamma(\pi-\gamma)}{2\left(\log(R\mu^{(\pi-\gamma)/2\pi}) + \frac{\pi-\gamma}{2\pi}\log\frac{8\pi^2}{\beta^2} + 2C\right)^2} \tag{B.9}$$

in agreement with the analytic continuation of equation (18).

References

[1] Yang C N and Yang C P 1969 *J. Math. Phys.* **10** 1115
[2] Zamolodchikov Al B 1990 *Nucl. Phys.* B **342** 695
[3] Klassen T R and Melzer E 1990 *Nucl. Phys.* B **338** 485
Martins M J 1990 *Phys. Lett.* B **240** 404
Christe P and Martins M J 1990 *Mod. Phys. Lett.* A **5** 2189
Klassen T R and Melzer E 1991 *Nucl. Phys.* B **350** 635
Martins M J 1990 *Phys. Rev. Lett.* **65** 2091
Martins M J 1990 *Phys. Rev. Lett.* **65** 409
[4] Zamolodchikov Al B 1991 *Nucl. Phys.* B **358** 497–523
Martins M J 1991 *Phys. Lett.* B **257** 317–21
Martins M J 1991 *Phys. Rev. Lett.* **67** 419–21
[5] Zamolodchikov Al B 1991 *Nucl. Phys.* B **358** 524–46

[6] Arefyeva I Ya and Korepin V E 1974 *Pisma ZhETF* **20** 680
[7] Vergeles S N and Gryanik V M 1976 *Yad. Fiz.* **23** 1324
Schroer B, Truong T T and Weisz P H 1976 *Phys. Lett.* B **63** 422
[8] Blote H W, Cardy J L and Nightingale M P 1986 *Phys. Rev. Lett.* **56** 742
[9] Zamolodchikov Al B 1991 *Phys. Lett.* B **253** 391
[10] Zamolodchikov Al B 1991 *Nucl. Phys.* B **366** 122–34
[11] Zamolodchikov A B 1987 *Sov. J. Nucl. Phys.* **46** 1090
[12] Cardy J and Ludwig A 1987 *Nucl. Phys.* B **285** 687
[13] Kastor D A, Martinec E J and Shenker S H 1989 *Nucl. Phys.* B **316** 590
[14] Zamolodchikov A B 1987 *JETP Lett.* **46** 160
[15] Zamolodchikov A B 1986 *Pisma ZhETF* **43** 565